J. Iron Steel Res. Int. (2023) 30:2471–2481
https://doi.org/10.1007/s42243-023-01022-3

ORIGINAL PAPER

Influence of lanthanum on inclusions and as-cast microstructures in a low-alloy high-strength steel

Can Liu[1] · Ji Zhang[2] · Qiang Ren[3] · Li-feng Zhang[4]

Received: 9 October 2022 / Revised: 22 November 2022 / Accepted: 30 November 2022 / Published online: 6 July 2023

Abstract
Advanced high-strength steel ingots with total lanthanum (TLa) contents of 0, 15×10^{-6}, 86×10^{-6} and 360×10^{-6} were prepared through laboratory experiments. The modification of inclusions and the variation of the as-cast microstructure with the content of lanthanum in the high-strength steel were analyzed. The result showed that with the increase in the TLa content in the steel from 0 to 360×10^{-6}, the modification path of inclusions in the as-cast steel was Al_2O_3 and calcium aluminate → $LaAlO_3$ → La_2O_2S → La_2O_2S–La_2O_3. The addition of La in the high-strength steel significantly refined the solidification structures. With the increase in the TLa content in the steel from 0 to 360×10^{-6}, the ratio of the equiaxed crystal region in the macrostructure increased from 30.1% to 50.7%, the proportion of the high-angle grain boundary in the microstructure increased from 36.9% to 69.8%, and the area fraction of the acicular ferrite and the bainite increased from 0 to 93.3%. Inclusions of $LaAlO_3$, La_2O_2S and La_2O_3 in the La-containing steel could act as heterogeneous nucleation cores of α-Fe during the solidification. With the increase in the TLa content in the steel, the number density of inclusions that could act as effective heterogeneous nucleation cores in the steel gradually increased, which enlarged the ratio of the equiaxed crystal region and the proportion of intragranular acicular ferrite, and refined the as-cast microstructure of the high-strength steel.

Keywords Advanced high-strength steel · Lanthanum · Inclusion · Heterogeneous nucleation · As-cast microstructure

1 Introduction

Traditional low-alloy high-strength steels are based on plain carbon steels, with a small number of microalloying elements such as Nb, V, Ti and Mo. A good combination of strength and toughness of the steel is able to be achieved through fine grain strengthening and precipitation strengthening [1–4]. With the increasing demand for high-performance steel materials, the advanced high-strength steel (AHSS) is developed. Compared with the traditional low-alloy high-strength steel whose microstructure is mainly ferrite, multiphase microstructures including ferrite, martensite, bainite and retained austenite were obtained through cooling control and further increased the mechanical performance of AHSS due to phase transformation strengthening [5–7]. Previous researches [8–10] on advanced high-strength steels mainly focused on the subsequent rolling and cooling control process, and the grain refinement of steel could be realized by thermo-mechanical process. The refined structure has a direct influence on the

✉ Qiang Ren
renqiang@ysu.edu.cn

✉ Li-feng Zhang
zhanglifeng@ncut.edu.cn

Can Liu
liucan_okay@163.com

Ji Zhang
ustbzhangji@163.com

[1] School of Materials Science and Engineering, Yanshan University, Qinhuangdao 066004, Hebei, China

[2] School of Metallurgical and Ecological Engineering, University of Science and Technology Beijing (USTB), Beijing 100083, China

[3] School of Mechanical Engineering, Yanshan University, Qinhuangdao 066004, Hebei, China

[4] School of Mechanical and Materials Engineering, North China University of Technology, Beijing 100144, China

rolling and forging process; thus, the as-cast structure refinement of high-strength steels is one of the key points to control the quality of the steel [11–13]. However, the study on the application of rare earth elements in high-strength steels to refine the structure before rolling was rarely reported.

In recent years, rare earth elements have been widely used in the cast steel, carbon steel and other industrial steels for their important role in improving the cleanliness of the steel [14, 15], the modification of inclusions [16–18] and microalloying [19, 20]. The solidification structure of the steel could be refined through the modification of inclusions and microalloying of rare earth elements in the steel. Bartlett and Avila [21] proposed that modified inclusions by cerium in a high-strength cast steel could act as heterogeneous nucleation cores for the primary formed γ phase, refining austenite grains from 10–12 mm to 100 μm. Xu et al. [22] found that the equilibrium distribution coefficient of cerium was small, and the solubility of rare earth inclusions in the liquid phase was larger, resulting in the enrichment of inclusions in the front of the liquid phase to affect the composition supercooling and inhibit the growth of grains. Wang [23] found that lanthanum could improve the supercooling of the steel and La-containing inclusions could serve as heterogeneous nucleation cores for δ ferrite to refine the as-cast structure of ASTM A216 steel. However, previous studies still lacked direct and accurate experimental basis.

In the current study, the effect of lanthanum contents on inclusions and as-cast microstructure of a high-strength low-alloy steel was investigated. Inclusions and as-cast microstructure in steels with various contents of lanthanum were analyzed. Thermodynamic analysis and two-dimensional lattice mismatch calculations were performed. The mechanism of the microstructure refinement by lanthanum addition was proposed.

2 Laboratory experiments and analysis

2.1 Experimental procedure

A slab of a commercial grade advanced high-strength steel with the composition listed in Table 1 was used as the raw material. During the experiment, a certain mass of slab specimens were put into a MgO crucible and then, melted using a vacuum induction furnace at 1600 °C. The schematic diagram of the vacuum induction furnace is shown in Fig. 1. After the slab was melted, a certain mass of LaFe alloys packed in a pure iron bag were added into the molten steel through the feeding bin. After three minutes after the addition of the LaFe alloy, the molten steel was poured into a cast iron ingot mold and was cooled to room temperature in the furnace. Four groups of experiments were performed and specimen with the total lanthanum (TLa) contents of 0, 15×10^{-6}, 86×10^{-6} and 360×10^{-6} were obtained. The measured contents of TLa in the steel and its standard deviation are listed in Table 2.

2.2 Analysis methods

The schematic diagram of the specimen preparation and analysis is shown in Fig. 2. The diameter and height of the ingot was approximately 55 and 90 mm, respectively, and the mass was around 1.8 kg. The ingot specimen was cut longitudinally from the middle, and the solidification structure of the longitudinal ingot section was etched using the corrosive solution with hydrochloric acid/deionized water of 1:1. After the distinguishment of the columnar crystal and the equiaxed crystal of the solidification structure, areas of different crystal regions in the

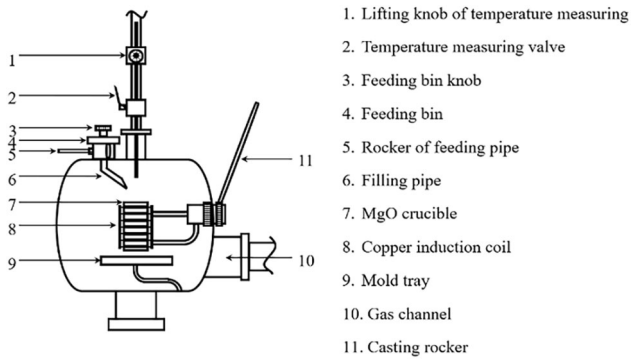

Fig. 1 Schematic diagram of vacuum induction furnace

Table 2 Contents of TLa in steel and its standard deviation

No.	TLa	Standard deviation
1	0	–
2	15×10^{-6}	0.4
3	86×10^{-6}	0.9
4	360×10^{-6}	1

Table 1 Chemical compositions of low-alloy high-strength steel (wt.%)

C	Si	Mn	P	Cr	Nb	Al	Ti	S	Fe
0.0476	0.6353	1.6822	0.0135	0.4939	0.0506	0.0487	0.0833	0.0009	Balance

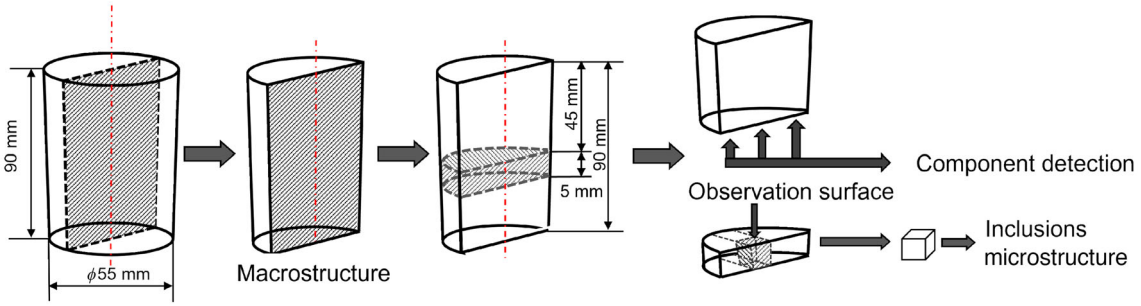

Fig. 2 Schematic diagram of specimen preparation and analysis

solidification structure and those of polygonal ferrite (PF), intragranular acicular ferrite (IGAF) and granular bainite ferrite (GBF) in the microstructure were measured using ImageJ software. The ratio of the equiaxed crystal region of the solidification structure of high-strength steels with different La contents was calculated. The content of the total lanthanum steel was analyzed using ICP-MSC. The size, chemical composition and number of inclusions in the steel with different TLa contents were analyzed using an automated inclusion in the analysis system equipped on a field-emission scanning election microscope (FE-SEM), ZEISS-Sigma 300. The minimum size for the analyzed inclusion was 1 μm. The orientation of the microstructure was examined using HITACHI SU-5000 field emission electron microscope equipped with electron backscattering (EBSD) under 30 kV and 20 mA working current.

3 Influence of lanthanum on macrostructure of steel

Figure 3 shows the macrostructure of high-strength steel ingots with different TLa contents. During the solidification process, the liquid phase gradually solidified from the outside region to the inside region of the ingot; meanwhile, the volume of the steel gradually decreased and there would not be enough liquid phase to fill the volume gaps in the late stage of solidification; thus, voids were formed in the center of the ingot. In the current paper, the voids in the ingot were not considered during the statistics of the macrostructure of ingots. The red line in Fig. 3 represented the boundary between the columnar crystal region and the equiaxed crystal region. Statistical results of the equiaxed crystal ratio of the high-strength steel with different TLa contents are shown in Fig. 4. With the increase in the TLa content in the steel from 0 to 360×10^{-6}, the equiaxed crystal ratio of the macrostructure gradually increased from 30.1% to 50.7%, and the macrostructure of the steel was obviously improved by the addition of La.

4 Influence of lanthanum on microstructural of steel

Figure 5 shows the microstructure of the high-strength steel with different lanthanum contents. In the steel without lanthanum addition, the main microstructure of the steel was PF. In the steel with 15×10^{-6} lanthanum, the microstructure was refined and was composed of 64.3% PF and 35.7% IGAF. The IGAF appeared in the steel, the PF was refined and its area fraction was reduced to 64.3%; besides, the proportion of the IGAF was 35.7%. When the

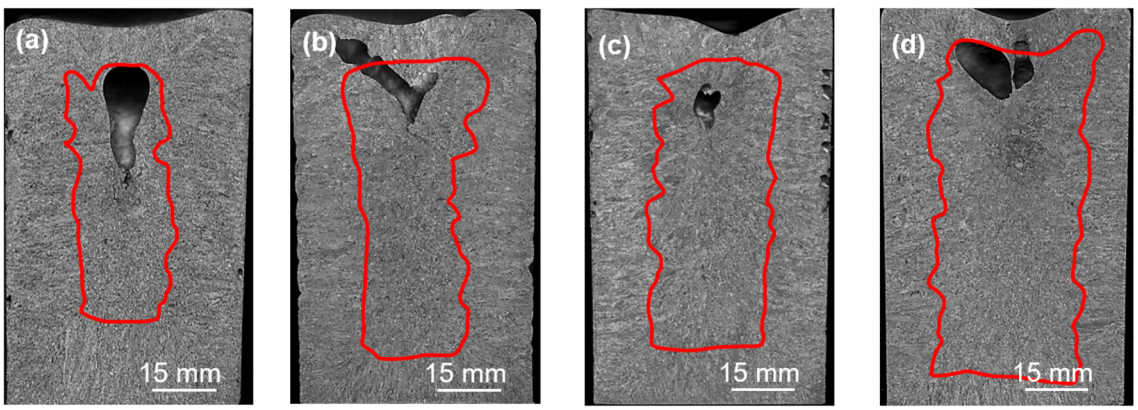

Fig. 3 Macrostructures of high-strength steel ingots with different TLa contents. **a** 0 La; **b** 15×10^{-6} La; **c** 86×10^{-6} La; **d** 360×10^{-6} La

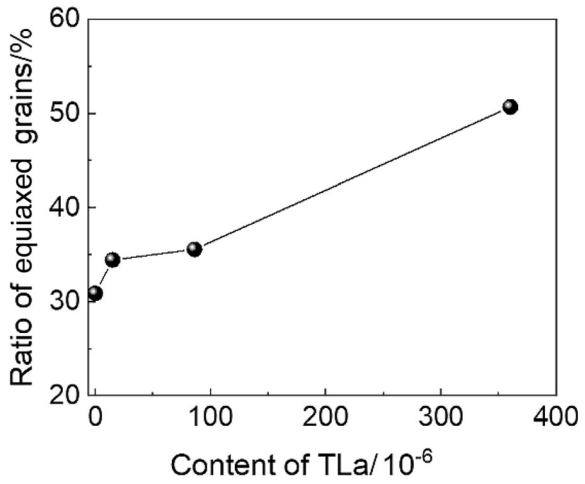

Fig. 4 Statistical results of equiaxed crystal ratio of high-strength steel with different La contents

content of lanthanum was 86 × 10^{-6}, the microstructure of the steel was composed of PF, IGAF and GBF. The content of the PF was further reduced to 33.7%, and the remaining microstructure was composed of GBF and IGAF accounting for 66.3%. As the content of lanthanum continuously increased to 360 × 10^{-6}, the area fraction of GBF and IGAF increased to 93.3%. It can be concluded that the proportion of IGAF and GBF increased while that of PF decreased with the increase in the lanthanum content, which was caused by the increase in the phase transformation activation energy of PF after the addition of lanthanum, thereby, inhibiting the formation and growth of PF [24]. Acicular ferrite (AF) and bainite ferrite (BF) coexisted in the steel after the furnace cooling, both of which were transformed at the medium temperature. Besides, the formation of rare earth inclusions in the steel with lanthanum addition provided enough heterogeneous nucleation sites for AF and BF during the transformation process [25, 26]. The structure of AF is α-Fe and BF is a multi-phase composed of α-Fe and Fe_3C. La-containing inclusions could induce the heterogeneous nucleation of α-Fe, as shown in Fig. 6. Thus, after the addition of La in the steel, La-containing inclusions were formed, which facilitated the heterogeneous nucleation and growth of AF and BF. The possibility for La-containing inclusions to induce heterogeneous nucleation of ferrite is discussed in Sect. 6.

To further analyze the orientation of the microstructure in steel, EBSD and orientation difference analyses of the high-strength steel with different La contents were carried out. As shown in Fig. 7, lanthanum had a great influence on the ratio of high-angle grain boundaries ($\theta > 15°$) in the orientation difference distribution, where θ is the angle between two crystal orientations. As shown in Fig. 8, the variation in the ratio of high-angle grain boundaries in the steel showed a single nonlinear increase trend with the increase in the lanthanum content, and compared with the steel with 15 × 10^{-6} lanthanum, low-angle boundaries increased and high-angle boundaries decreased when the lanthanum content was 86 × 10^{-6}, resulting in the inflection point when the lanthanum content in the steel was 86 × 10^{-6}. Previous studies found that acicular ferrite could form interlocking structures with high-angle grain boundaries in the steel [27], and a large number of smaller-

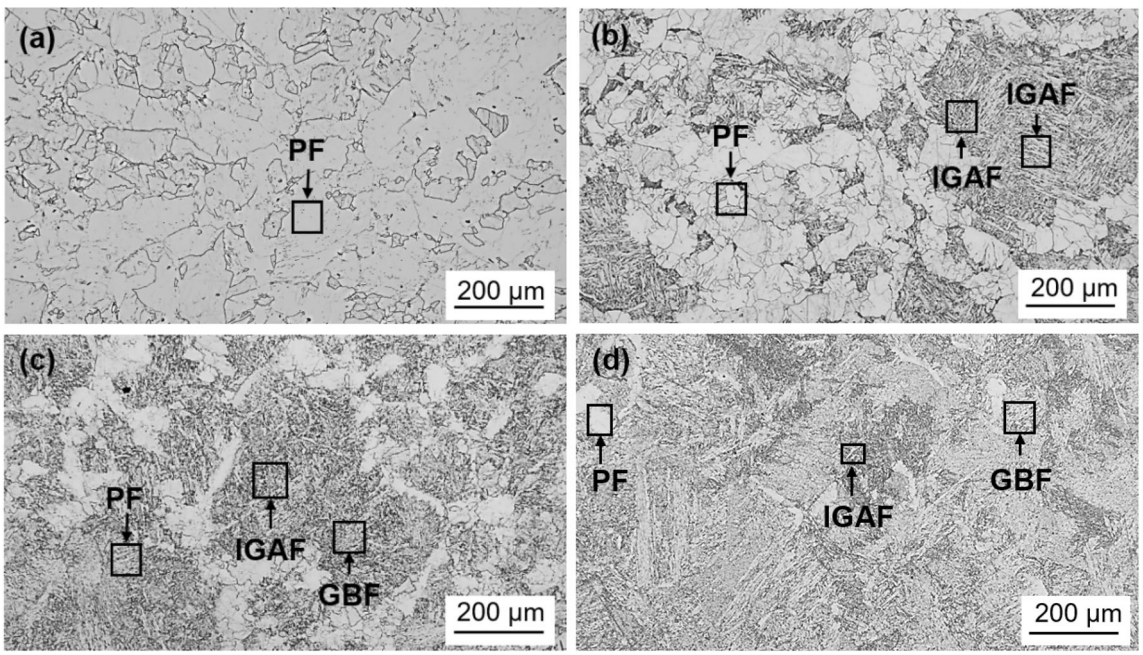

Fig. 5 Microstructure of high-strength steel with different TLa contents. **a** 0 La; **b** 15 × 10^{-6} La; **c** 86 × 10^{-6} La; **d** 360 × 10^{-6} La

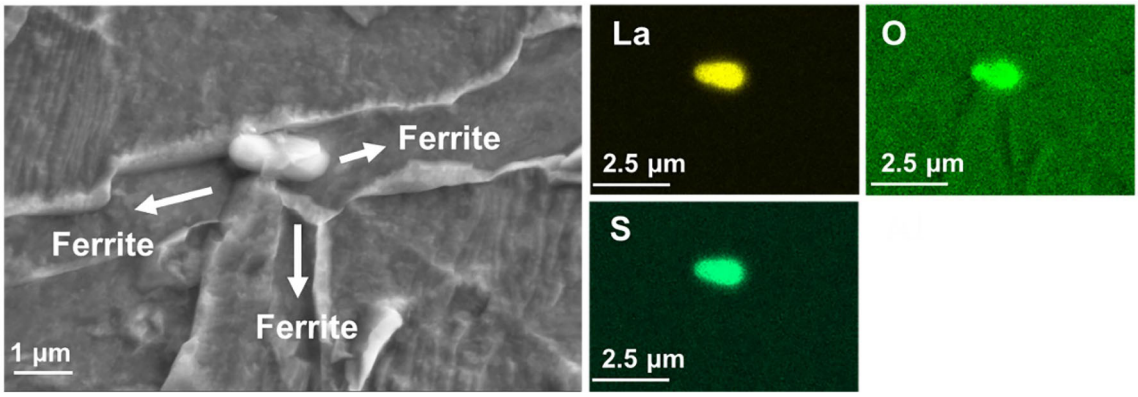

Fig. 6 Heterogeneous nucleation of ferrite induced by La-containing inclusions

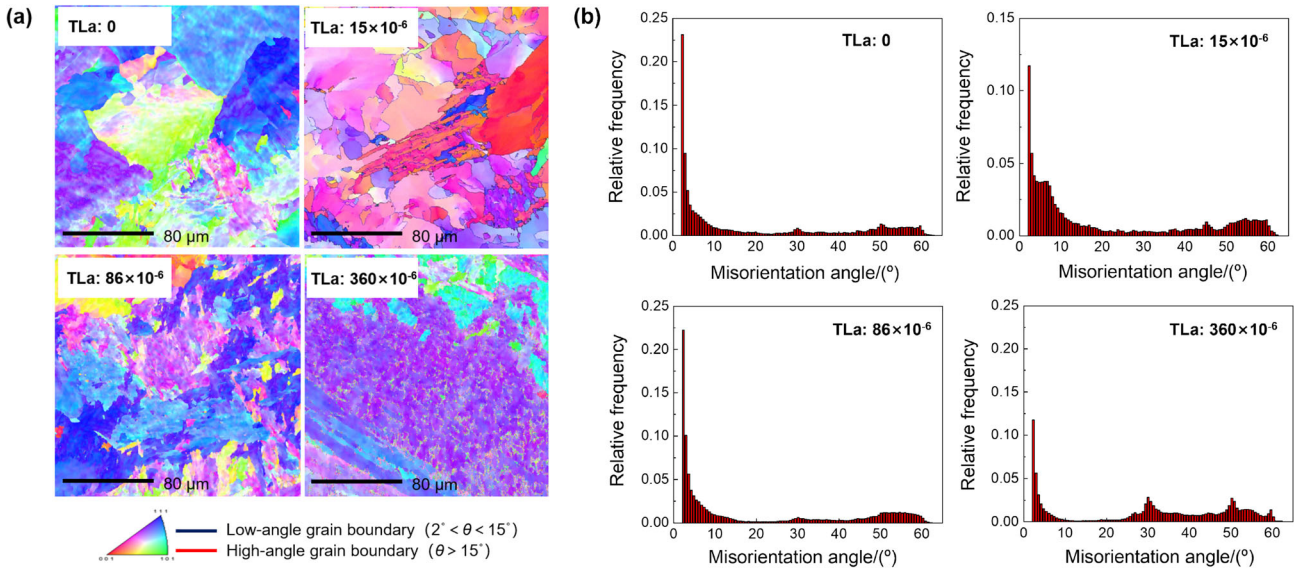

Fig. 7 EBSD scanning results (**a**) and misorientation distributions (**b**) in microstructure of high-strength steels with different TLa contents

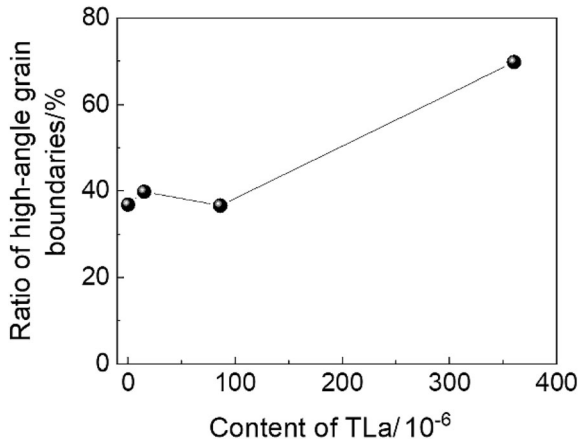

Fig. 8 Variation of high-angle grain boundaries ratio with TLa contents in steel

size martensite/austenite islands (M/A islands) in GBF could increase the interface between the M/A islands and ferrite which would increase the orientation difference, leading to the increase in the high-angle boundaries ratio [28]. On the contrary, when the size of the M/A islands was large and the interface between the M/A islands and ferrite was small, the ratio of high-angle boundaries could not be increased even if the granular bainite existed in the steel. As shown in Fig. 5, when the content of lanthanum was in the range between 0 and 86×10^{-6}, the structure was refined but the fraction of high-angle boundaries was not improved. When the content of lanthanum was 360×10^{-6}, both the structure was refined and the fraction of high-angle boundaries was improved, which may be related to M/A islands with bigger size in the steel with 86×10^{-6} lanthanum.

5 Inclusions in steel

Figure 9 shows the elemental mapping of typical La-containing inclusions in the high-strength steel with different TLa contents. When the content of TLa in the steel was 0, inclusions consisted of composite inclusions with Al_2O_3 or calcium aluminate as the core and TiN wrapping around it. In the steel with 15×10^{-6} La, the oxide core of Al_2O_3 and calcium aluminate was modified into $LaAlO_3$. As the content of TLa in the steel increased into 86×10^{-6}, inclusions were further transformed into La_2O_2S and La_2O_3. When the content of TLa in the steel was 360×10^{-6}, inclusions were mainly La_2O_2S and composite inclusions with La_2O_2S as the core and La_2O_3 wrapping around it.

Variations of the number density of different kinds of inclusions, the composition, area fraction and number density of total inclusions in the steel with the TLa content are shown in Fig. 10. Inclusions in the steel without La were mainly TiN. When the mass fraction of the TLa content in the steel was 360×10^{-6}, the inclusions were finally modified into La_2O_2S and La_2O_3. With the increase

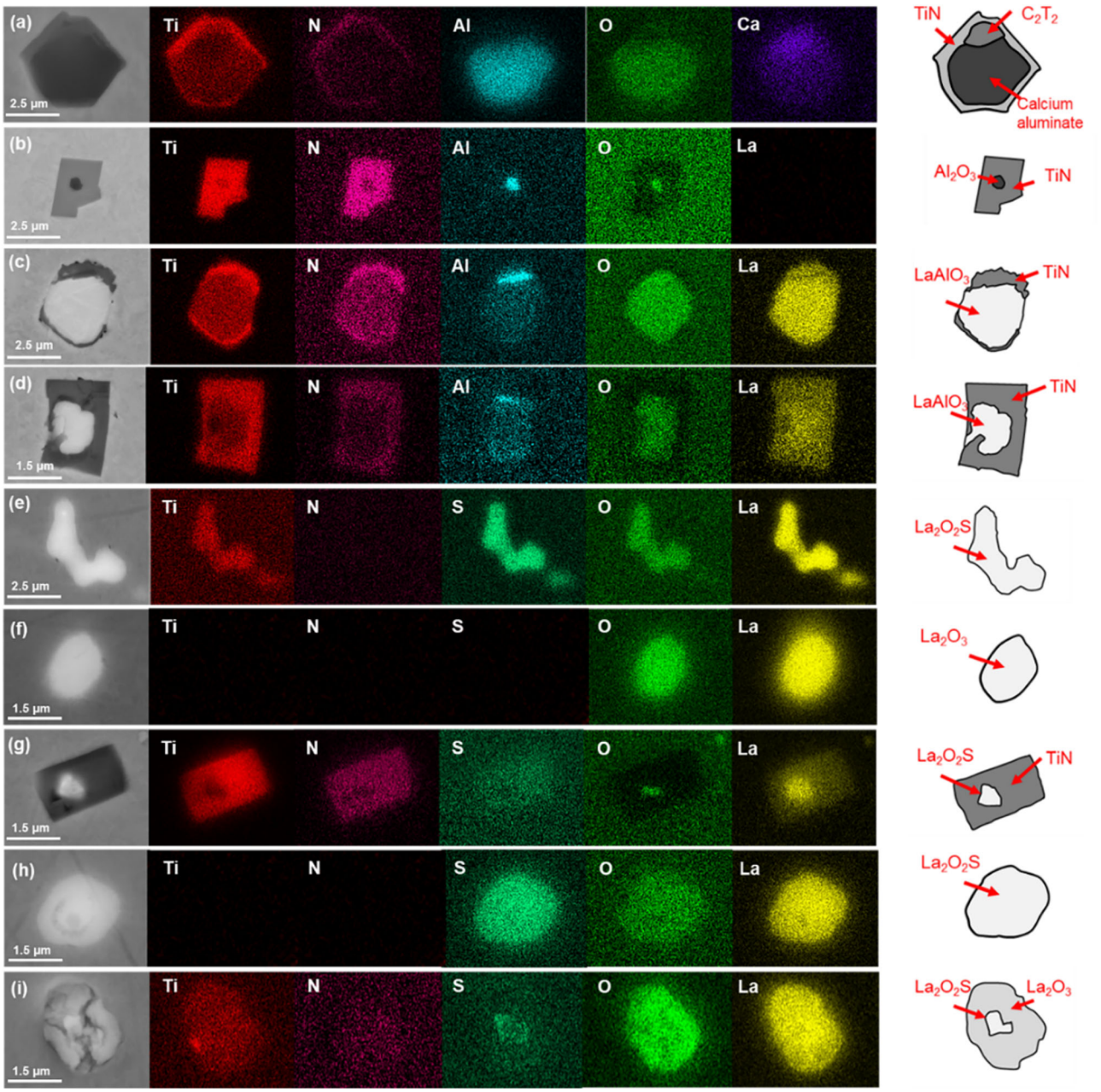

Fig. 9 Elemental mapping of typical La-containing inclusions in high-strength steel with different La contents. **a**, **b** 0 La; **c**, **d** 15×10^{-6} La; **e**–**g** 86×10^{-6} La; **h**, **i** 360×10^{-6} La

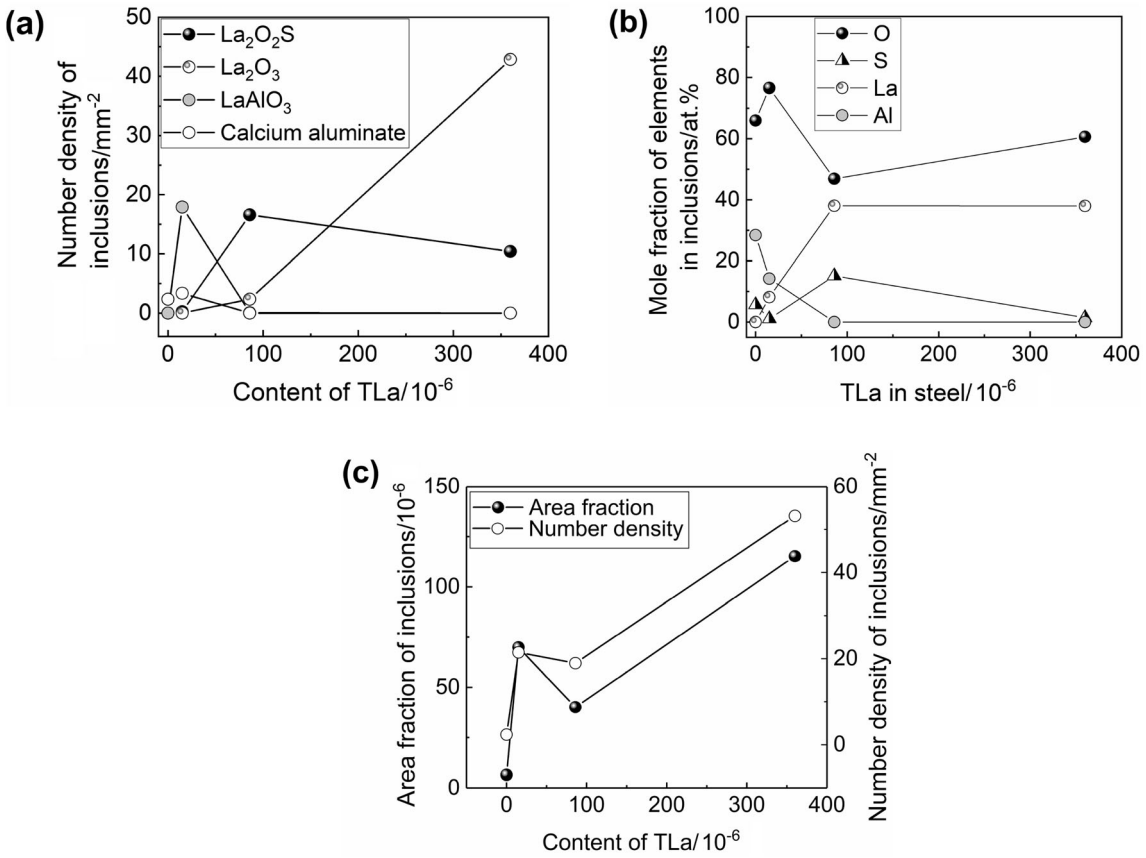

Fig. 10 Effect of TLa content on number density of different kinds of inclusions (**a**), composition (**b**), area fraction and number density of inclusions in steel (**c**)

in the TLa content in the steel from 0 to 360 × 10^{-6}, the modification path of inclusions in the steel was Al_2O_3 and calcium aluminate → $LaAlO_3$ → La_2O_2S → La_2O_2S–La_2O_3. The number density and area fraction of inclusions showed an increasing tendency with the increase in the TLa content in the steel. When the TLa content increased from 15 × 10^{-6} to 360 × 10^{-6}, the number density and area fraction of inclusions first decreased and then, increased, and reached the minimum value which were 18.98 mm^{-2} and 40.12 × 10^{-6}, respectively, when the TLa content in the steel was 86 × 10^{-6}.

Transformation of inclusions in the steel with different TLa contents during the solidification process was calculated using FactSage 7.1 with databases of FactPS, FToxid, FSstel and a private database containing the thermodynamic data of La_2O_2S, as shown in Fig. 11. Figure 11a shows the total amount variation of inclusions with the content of lanthanum in the steel, and the total amount of inclusions showed an increasing tendency with the increase in the lanthanum content in the steel. Variations of inclusions composition with the content of lanthanum in the steel are shown in Fig. 11b and c, and initial calcium aluminate and alumina in the steel were gradually modified into lanthanum-containing inclusions with the increase in the lanthanum content in the steel. Combined the experimental results with the results shown in Fig. 10, for the steel without La, inclusions in the steel after solidification were mainly calcium aluminates and Al_2O_3, which was consistent with the result shown in Fig. 9a and b. In the steel with the TLa content of 15 × 10^{-6}, inclusions in the solid steel were mainly $LaAlO_3$, which was in consistence with the result shown in Fig. 9c and d. In the steel with 86 × 10^{-6} lanthanum, inclusions were mainly La_2O_2S, which roughly agreed with the result shown in Fig. 9e–g. In the steel with 360 × 10^{-6} lanthanum, inclusions were mainly La_2O_2S and La_2O_3, which was in consistence with the result shown in Fig. 9h and i.

6 Heterogeneous nucleation of ferrite induced by inclusions

Inclusions in the steel can act as effective heterogeneous nucleation cores during solidification of steels to reduce the activation energy barrier of nucleation, promoting the nucleation of the first precipitated phase of steel, and

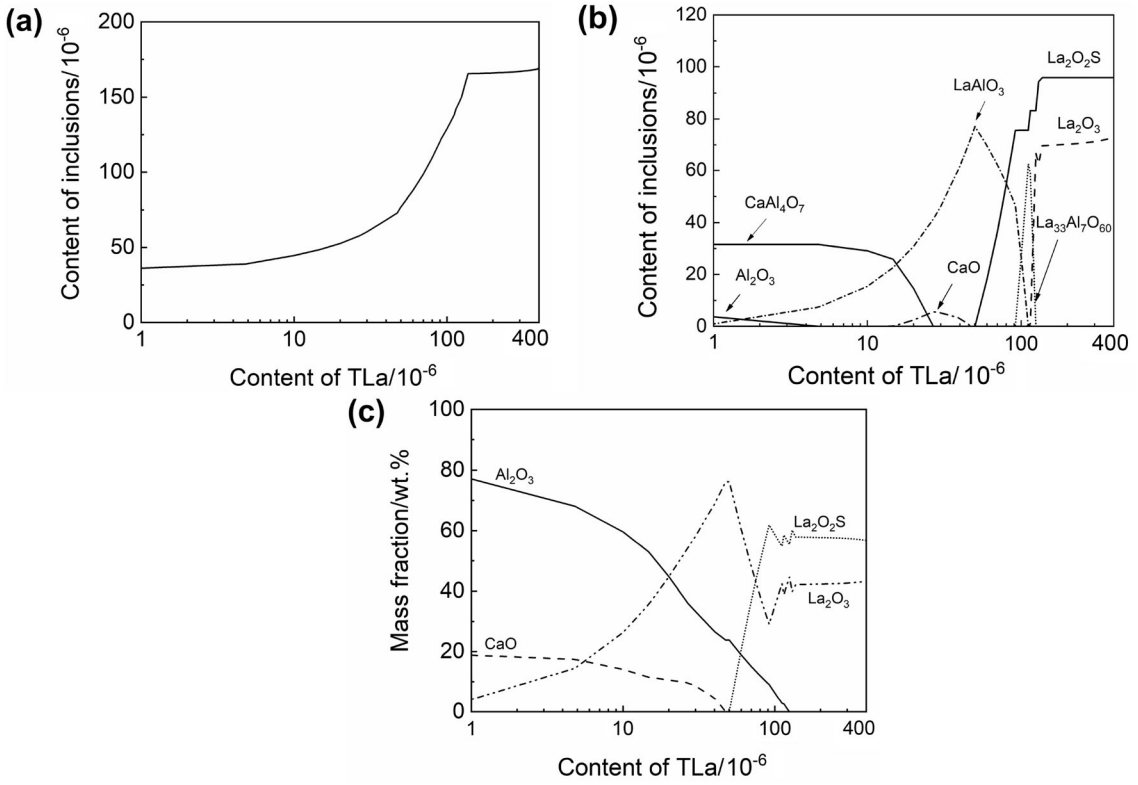

Fig. 11 Variations of inclusions composition with TLa content in steel. **a** Total content of inclusions; **b** content of each type of inclusion; **c** average composition of inclusions

Table 3 Lattice parameters of different inclusions and α-Fe

Inclusions	Space group	*a*/Å	*b*/Å	*c*/Å	α/(°)	*β*/(°)	*γ*/(°)	Reference
La_2O_2S	$P\bar{3}m1$	3.927	3.927	6.768	90	90	120	[30]
$LaAlO_3$	$R\bar{3}H$	5.381	5.381	13.174	90	90	120	[31]
La_2O_3	P_{63}/mmc	4.057	4.057	6.430	90	90	120	[32]
α-Fe	$Im\bar{3}m$	2.850	2.850	2.850	90	90	90	[33]

a, *b*, *c*—Cell edge length; α, *γ*, *β*—angle between cell edge

refining the as-cast structure of the steel. The mismatch between inclusion and the matrix can reveal the grain refinement phenomenon [21].

Bramfitt [29] proposed a calculation method of the two-dimensional mismatch degree, as shown in Eq. (1). When the mismatch degree was less than 6%, the heterogeneous nucleation effect was the best; when the mismatch degree was between 6% and 12%, the heterogeneous nucleation effect was relatively poor; when the mismatch degree was more than 12%, the heterogeneous nucleation cannot be induced.

$$\delta_{(hkl)_n}^{(hkl)_s} = \sum_{i=1}^{3} \frac{\left| d_{[uvw]_s^i} \cos\theta - d_{[uvw]_n^i} \right|}{d_{[uvw]_n^i}} \times 100 \quad (1)$$

where $(hkl)_s$ is the low exponential plane of the base; $(hkl)_n$ is the low index plane of nucleation phase; $[uvw]_s$ is the low index crystal orientation of $(hkl)_s$; $[uvw]_n$ is the low index crystal orientation of $(hkl)_n$; d[uvw]$_s$ is the atomic spacing along the $[uvw]_s$ crystal direction; $d[uvw]_n$ is the atomic spacing along the $[uvw]_n$ crystal direction; and i is one of the three lowest index directions within a 90° quadrant of the planes of the nucleated inclusion and the substrate.

Lattice parameters of different kinds of inclusions and α-Fe are shown in Table 3, and minimum values of mismatch degrees are shown in Table 4. Relationship of crystallizing planes between La_2O_2S, $LaAlO_3$, La_2O_3 and α-Fe is shown in Fig. 12. The optimum mismatch degree between La_2O_2S, $LaAlO_3$, La_2O_3 and α-Fe was 2.6%,

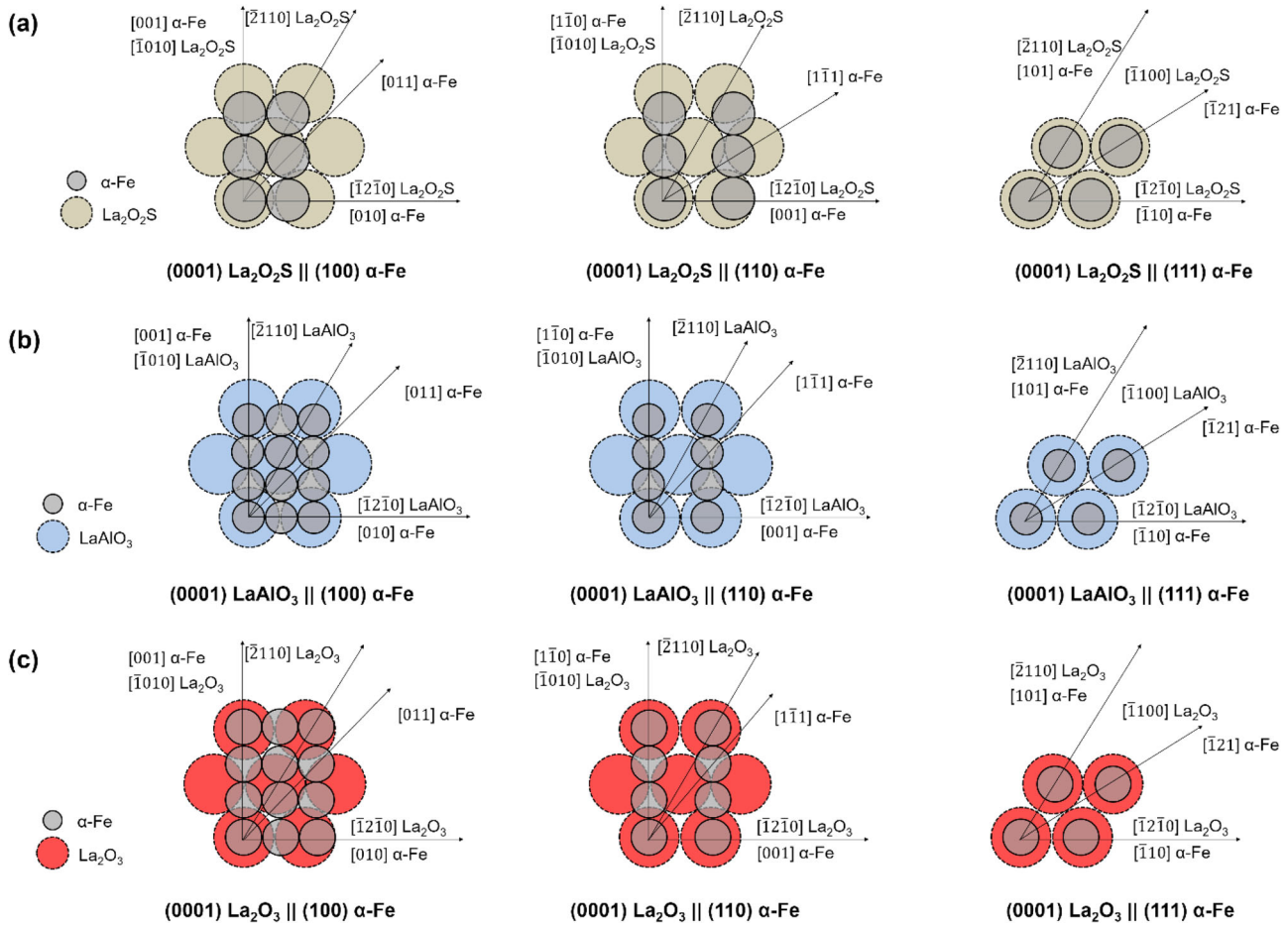

Fig. 12 Relationship of crystallizing planes between La_2O_2S (**a**), $LaAlO_3$ (**b**), La_2O_3 (**c**) and α-Fe

8.4%, and 0.7%, respectively. The mismatch degrees between La_2O_3, La_2O_2S and α-Fe were all less than 6%, indicating that both La_2O_3 and La_2O_2S were most conducive to induce heterogeneous nucleation of α-Fe. The mismatch between $LaAl_2O_3$ and α-Fe was 8.4%, which was between 6% and 12%, and the induction ability for heterogeneous nucleation was relatively poor. In the steel with La addition, $LaAlO_3$, La_2O_2S and La_2O_3 could act as heterogeneous nucleation cores of α-Fe during solidification. When the content of TLa was not higher than 86×10^{-6}, the nucleation of ferrite and refinement of grains was mainly related to $LaAlO_3$ and La_2O_2S during the solidification process. When the TLa content was 360×10^{-6}, the content of La_2O_3 in inclusions was higher, which plays the dominant role in the nucleation of ferrite and refinement of grains.

To further illustrate the influence of the interaction between La-containing inclusions and ferrite nucleation on the microstructure, according to Fig. 10c. The number density of La-containing inclusions with strong heterogeneous' nucleation ability increased nonlinearity with the increase in the TLa content in the steel and an inflection point appeared when the TLa content was 86×10^{-6}. In Sects. 3 and 4, it was also found that the TLa content increased from 15×10^{-6} to 86×10^{-6}, the change in the equiaxed crystal ratio of the solidification macrostructure (as shown in Fig. 4) and the change of high-angle grain boundaries (as shown in Fig. 7) varied little when the TLa content increased from 15×10^{-6} to 86×10^{-6}. It was because when the TLa content was 86×10^{-6}, the inclusions mainly existed in chain shape. Figure 13 shows the three-dimensional morphology of chain inclusions. Because of the limited nucleation site and the aggregation of La-containing inclusions, the number density of inclusions was greatly affected. At the same time, the aggregation of La-containing inclusions reduced the crystal planes that could match acicular ferrite to a certain extent, resulting in little change in the equiaxed crystal ratio, inapparent refinement of the microstructure and slight decrease in the high-angle grain boundaries fraction when the TLa content in the steel increased from 15×10^{-6} to 86×10^{-6}. The aggregation of inclusions could inevitably increase the inclusions size, which would lead to the deterioration of the steel property. Therefore, the average

Table 4 Mismatch degree between different inclusions and α-Fe

Inclusion type	Crystal plane	θ/(°)	Mismatch degree/%
La_2O_2S	(0001)La_2O_2S ‖ (100)α-Fe	3.69	25.1
	(0001)La_2O_2S ‖ (110)α-Fe	4.76	13.4
	(0001)La_2O_2S ‖ (111)α-Fe	0	2.6
$LaAlO_3$	(0001)$LaAlO_3$ ‖ (100)α-Fe	9.74	8.4
	(0001)$LaAlO_3$ ‖ (110)α-Fe	0	24.3
	(0001)$LaAlO_3$ ‖ (111)α-Fe	9.74	42.9
La_2O_3	(0001)La_2O_3 ‖ (100) α-Fe	15	10.5
	(0001)La_2O_3 ‖ (110) α-Fe	4.76	11.0
	(0001)La_2O_3 ‖ (111) α-Fe	0	0.7

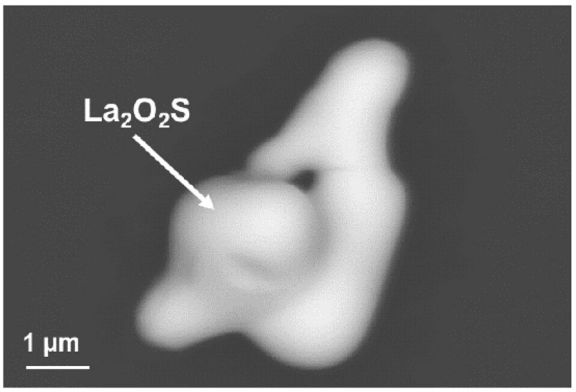

Fig. 13 Three-dimensional morphologies of chain inclusions in steel with 86 × 10^{-6} La

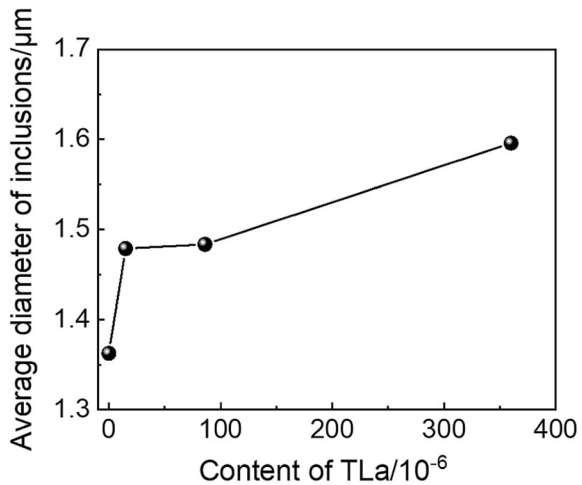

Fig. 14 Average diameter of rare earth containing inclusions in steel

diameter of rare earth containing inclusions in the steel was calculated, as shown in Fig. 14. The average diameter of rare earth containing inclusions changed little under different La additions, that is, chain inclusions were the aggregation of smaller-size inclusions, and the influence on the size of rare earth inclusions can be ignored in this experiment.

7 Conclusions

1. With the increase in the TLa content in the high-strength steel from 0 to 360 × 10^{-6}, the modification paths of inclusions in the steel were Al_2O_3 and calcium aluminate → $LaAlO_3$ → La_2O_2S → La_2O_2S–La_2O_3.
2. The addition of La in the high-strength steel significantly improved its solidification structure. As the content of TLa in the steel increased from 0 to 360 × 10^{-6}, the equiaxed crystal ratio of solidification macrostructure increased from 30.1% to 50.7%, the proportion of high-angle grain boundaries in the microstructure increased from 36.9% to 69.8%, and the total area fraction of acicular ferrite and bainite increased from 0 to 89.8%.
3. In the steel with La addition, $LaAlO_3$, La_2O_2S and La_2O_3 inclusions could act as heterogeneous nucleation cores of α-Fe. With the increase in the TLa content, the number density of inclusions in the steel that can effectively induce heterogeneous nucleation gradually increased, which was beneficial to refining the as-cast structure of the high-strength steel, and finally increased the proportion of acicular ferrite, granular bainite ferrite and the equiaxed crystal ratio of the solidification macrostructure.

Acknowledgements The authors are grateful for the support from S&T Program of Hebei (Grant No. 20311004D), the National Natural Science Foundation of China (Grant Nos. U22A20171 and 52104342), the Natural Science Foundation of Hebei Province (Grant No. E2021203062), the High Steel Center (HSC) at Yanshan University, Hebei Innovation Center of the Development and Application of High Quality Steel Materials, and Hebei International Research Center of Advanced and Intelligent Manufacturing of High Quality Steel Materials.

Declarations

Conflict of interests The authors have no competing interests to declare that are relevant to the content of this article.

References

[1] D. Rasouli, S.K. Asl, A. Akbarzadeh, G.H. Daneshi, Mater. Des. 30 (2009) 2167–2172.
[2] Y. Zhi, X.H. Liu, Z.F. Wang, Adv. Mater. Res. 418–420 (2011) 1622–1628.
[3] N. Isasti, D. Jorge-Badiola, M.L. Taheri, B. López, P. Uranga, Metall. Mater. Trans. A 42 (2011) 3729–3742.
[4] Y. Hou, G. Cheng, ISIJ Int. 58 (2018) 2298–2307.

[5] R.G. Davies, Metall. Mater. Trans. A 9 (1978) 41–52.
[6] A. Kumar, S.B. Singh, K.K. Ray, Mater. Sci. Eng. A 474 (2008) 270–282.
[7] D.I. Hyun, S.M. Oak, S.S. Kang, Y.H. Moon, J. Mater. Process. Technol. 130–131 (2002) 9–13.
[8] M. Janošec, I. Schindler, J. Palát, L. Čížek, V. Vodárek, E. Místecký, M. Růžička, L.A. Dobrzański, S. Rusz, P. Suchánek, J. Achiev. 20 (2007) 251–254.
[9] J. Speer, D.K. Matlock, B.C. De Cooman, J.G. Schroth, Acta Mater. 51 (2003) 2611–2622.
[10] R. Song, D. Ponge, D. Raabe, J.G. Speer, D.K. Matlock, Mater. Sci. Eng. A 441 (2006) 1–17.
[11] Y. Ji, M.X. Zhang, H. Ren, Metals 8 (2018) 884.
[12] B. Buchmayr, Steel Res. Int. 88 (2017) 1700182.
[13] H. Li, A. McLean, J.W. Rutter, I.D. Sommerville, Metall. Trans. B 19 (1988) 383–395.
[14] H. Wang, Y.P. Bao, M. Zhao, M. Wang, X.M. Yuan, S. Gao, Int. J. Miner. Metall. Mater. 26 (2019) 1372–1384.
[15] Y.D. Li, C.J. Liu, C.L. Li, M.F. Jiang, J. Iron Steel Res. Int. 22 (2015) 457–463.
[16] Q. Ren, L. Zhang, Metall. Mater. Trans. B 51 (2020) 589–600.
[17] M. Nabeel, M. Alba, R. Karasev, P. Nsson, N. Dogan, Metall. Mater. Trans. B 50 (2019) 1674–1685.
[18] H. Torkamani, S. Raygan, C. Garcia-Mateo, J. Rassizadehghani, Y. Palizdar, D. San-Martin, Metall. Mater. Trans. A 49 (2018) 4495–4508.
[19] G. Li, P. Lan, J. Zhang, G. Wu, Metall. Mater. Trans. B 51 (2020) 452–466.
[20] C. Liu, R.I. Revilla, Z. Liu, D. Zhang, X. Li, H. Terryn, Corros. Sci. 129 (2017) 82–90.
[21] L.N. Bartlett, B.R. Avila, Int. J. Met. 10 (2016) 401–420.
[22] J. Xu, G. Qi, J. Zhu, B. Xu, K. Zhang, L. Wang, J. Rare Earths. 24 (2006) 486–489.
[23] A.Q. Wang, Kem. Ind. 65 (2016) 11–16.
[24] W. Lu, L. Zhang, Z. Xu, J. Iron Steel Res. Int. 28 (1993) 62–86.
[25] H.L. Liu, C.J. Liu, M.F. Jiang, Mater. Des. 33 (2012) 306–312.
[26] Y.P. Ji, Y.M. Li, M.X. Zhang, W. Qu, T.X. Zhao, H.P. Ren, Metall. Mater. Trans. A 51 (2020) 1707–1718.
[27] L.C. An, J. Cao, L.C. Wu, H.H. Mao, Y.T. Yang, J. Iron Steel Res. Int. 23 (2016) 1333–1341.
[28] H. Fang, H. Deng, Mech Eng. 1 (1981) 7–16.
[29] B.L. Bramfitt, Metall. Trans. 1 (1970) 1987–1995.
[30] S. Zhukov, A. Yatsenko, V. Chernyshev, V. Trunov, E. Tserkovnaya, O. Antson, J. Hölsä, P. Baulés, H. Schenk, Mater. Res. Bull. 32 (1997) 43–50.
[31] H. Lehnert, H. Boysen, J. Schneider, F. Frey, D. Hohlwein, P. Radaelli, H. Ehrenberg, Zeitschrift Für Kristallographie Cryst. Mater. 215 (2000) 536–541.
[32] P. Aldebert, J.P. Traverse, Mater. Res. Bull. 14 (1979) 303–323.
[33] H. Saitoh, A. Machida, R. Iizuka-Oku, T. Hattori, A. Sano-Furukawa, K.I. Funakoshi, T. Sato, S.I. Orimo, K. Aoki, Sci. Rep. 10 (2020) 9934.